New H-mode regimes with small ELMs and high thermal confinement in the Joint European Torus

Document license:
TAVERNE

DOI:
[10.1063/5.0072236](10.1063/5.0072236)

Document status and date:
Published: 01/03/2022

Document Version:
Publisher's PDF, also known as Version of Record (includes final page, issue and volume numbers)

Please check the document version of this publication:

• A submitted manuscript is the version of the article upon submission and before peer-review. There can be important differences between the submitted version and the official published version of record. People interested in the research are advised to contact the author for the final version of the publication, or visit the DOI to the publisher's website.
• The final author version and the galley proof are versions of the publication after peer review.
• The final published version features the final layout of the paper including the volume, issue and page numbers.

Link to publication

Download date: 06. dic. 2023

🄳 J. Garcia, E. de la Luna, 🄳 M. Sertoli, et al.

COLLECTIONS

🄵 This paper was selected as Featured

View Online   Export Citation   CrossMark

ARTICLES YOU MAY BE INTERESTED IN

Influence of anomalous perpendicular transport on linear tearing mode dynamics in tokamak plasmas
Physics of Plasmas **29**, 032507 (2022); https://doi.org/10.1063/5.0082331

Ion thermal transport in the H-mode edge transport barrier on DIII-D
Physics of Plasmas **29**, 012506 (2022); https://doi.org/10.1063/5.0072155

Inverse Compton scattering of the ITG turbulence by energetic ions
Physics of Plasmas **29**, 030702 (2022); https://doi.org/10.1063/5.0083009

New H-mode regimes with small ELMs and high thermal confinement in the Joint European Torus Ⓕ

J. Garcia,[1,a] ⒾD E. de la Luna,[2] M. Sertoli,[3] ⒾD F. J. Casson,[3] S. Mazzi,[1,4] ⒾD Ž. Štancar,[5] G. Szepesi,[3] D. Frigione,[6]
L. Garzotti,[3] ⒾD F. Rimini,[3] D. van Eester,[7] ⒾD P. Lomas,[3] C. Sozzi,[8] N. Aiba,[9] M. Dicorato,[10] A. Mariani,[10] ⒾD R. Coelho,[11]
L. Frasinetti,[12] G. T. A. Huijsmans,[1,13] ⒾD F. Liu,[1] and JET Contributors[b]

AFFILIATIONS

[1]CEA, IRFM, F-13108 Saint Paul-lez-Durance, France
[2]Laboratorio Nacional de Fusión, CIEMAT, 28040 Madrid, Spain
[3]Culham Centre for Fusion Energy of UKAEA, Culham Science Centre, Abingdon OX14 3DB, United Kingdom
[4]Aix-Marseille Université, CNRS PIIM, UMR 7345, Marseille, France
[5]Jožef Stefan Institute, Jamova cesta 39, SI-1000 Ljubljana, Slovenia
[6]National Agency for New Technologies, Energy and Sustainable Economic Development, ENEA, C.R. Frascati, Roma 00044, Italy
[7]LPP-ERM/KMS, EUROfusion Consortium Member-Trilateral Euregio Cluster, Brussels 1000, Belgium
[8]Istituto per la Scienza e Tecnologia dei Plasmi, 20125 Milano, Italy
[9]National Institutes for Quantum and Radiological Science and Technology, Naka, Ibaraki 311-0193, Japan
[10]Istituto per la Scienza e Tecnologia dei Plasmi, CNR, via Cozzi 53, 20125 Milan, Italy
[11]Instituto de Plasmas e Fusão Nuclear, Instituto Superior Técnico, Universidade de Lisboa, 1049-001 Lisboa, Portugal
[12]Division of Fusion Plasma Physics, KTH Royal Institute of Technology, Stockholm 114 28, Sweden
[13]Eindhoven University of Technology, P.O. Box 513, 5600 MB Eindhoven, The Netherlands

[a]Author to whom correspondence should be addressed: jeronimo.garcia@cea.fr
[b]See the author list of "Overview of JET results for optimizing ITER operation" by J. Mailloux *et al.* to be published in Nuclear Fusion
Special issue: Overview and Summary Papers from the 28th Fusion Energy Conference (Nice, France, 10–15 May 2021).

ABSTRACT

New H-mode regimes with high confinement, low core impurity accumulation, and small edge-localized mode perturbations have been obtained in magnetically confined plasmas at the Joint European Torus tokamak. Such regimes are achieved by means of optimized particle fueling conditions at high input power, current, and magnetic field, which lead to a self-organized state with a strong increase in rotation and ion temperature and a decrease in the edge density. An interplay between core and edge plasma regions leads to reduced turbulence levels and outward impurity convection. These results pave the way to an attractive alternative to the standard plasmas considered for fusion energy generation in a tokamak with a metallic wall environment such as the ones expected in ITER.

Published under an exclusive license by AIP Publishing. https://doi.org/10.1063/5.0072236

INTRODUCTION

The construction of the tokamak ITER[1] will clarify the possibilities of nuclear fusion of deuterium (D) and tritium (T) by magnetically confined plasmas as a reliable source of energy. ITER operation will combine a significant number of challenges, such as the simultaneous requirements of high stability and confinement of plasmas. From present day experiments, it is well known that confined plasmas lead to instabilities of different natures, such as microturbulence or magnetohydrodynamics (MHD), which are generated by strong temperature and density gradients and that can severely degrade the thermal confinement. Furthermore, the presence of a metal wall generates high Z impurities that can be transported to the plasma core by such

gradients, polluting the plasma and generating unacceptable levels of radiated power, which can damage the plasma confinement and lead to disruptions.

The preferred mode of operation in ITER, the H-mode,[2] exemplifies such difficulties. Although the confinement is enhanced with respect to other operation regimes due to the build-up of the so-called pedestal at the plasma edge, i.e., a region where heat and particle transport is vastly suppressed, the strong gradient formed leads to MHD instabilities called Edge Localized Modes (ELMs).[3] ELMs result in the periodic, rapid expulsion of edge plasma, leading to erosion and thermal stresses of the plasma facing components. Simultaneously, experience in tokamaks shows that ELMs are beneficial for preventing impurity penetration in the plasma core, and in particular, in metal wall devices, they regularly flush the generated tungsten (W) from the plasma facing components when their frequency is high enough.[4,5] However, high-frequency ELMs, usually obtained in conditions of strong particle fueling by gas puff injection, lead to thermal energy confinement degradation.[5] Low neutral gas injection can be used to improve the confinement, but this typically leads to a strong reduction in the ELM frequency and, as a result, the beneficial effect of impurity flushing by ELMs is significantly reduced. This, in the presence of the metal wall, causes an increase in high Z impurity content in the core region, which often leads to a radiative collapse, increasing the risk of a plasma disruption.[6] Therefore, finding a plasma state with high thermal confinement, resilient to impurity accumulation with ELMs in a metal wall, has become a challenge in the magnetically confined fusion field.

In this paper, a new path toward edge plasma control and high thermal energy confinement is shown. Plasma regimes with small ELMs compatible with high core thermal energy confinement, fusion power, and low or absent impurity accumulation are found at the Joint European Torus (JET).[7] This is obtained through a regime involving the interplay between core and edge plasma regions in conditions close to the so-called baseline or inductive scenario,[8] which is the ITER main plasma operational regime. This represents an attractive alternative to other small ELMs regimes,[9–13] as these JET results are relevant for the initial ITER D–T phase, where the inductive scenario will be developed.

EXPERIMENTAL RESULTS

Recent experiments in JET have demonstrated new H-mode operating regimes with simultaneous access to small high-frequency ELMs and high thermal energy confinement, high D–D fusion reactions, and low high Z impurity accumulation in the plasma center, henceforth called Baseline Small ELM (BSE) regimes. The accessibility to such regime relies on the addition of high input power at high current and magnetic field and the optimization of the D neutral gas particle injection either by completely removing it or by partially replacing it with pellet injection.[14] Furthermore, the addition of small Ne quantities is observed to be beneficial for ensuring a stationary plasma. It is important to emphasize that the small ELMs observed in these new operating H-mode regimes achieved in JET have been obtained with simultaneously $q_{95} = 3.2$, $\beta_p < 1$, $H_{98}(y, 2) \sim 1.0$ and low pedestal collisonality, $\nu_e^* < 0.4$ (calculated following Ref. 12). This means that the BSE regime covers a different physics space than the other small ELM regimes obtained previously in ASDEX Upgrade (AUG-U),[11] EAST,[15] or JT-60U[9,16] and, therefore, may provide a new path to the initial D–T plasmas expected in ITER.[8] This can be clearly observed in Fig. 1, where two BSE plasmas, #94442 and #96994, are compared to other small ELM regimes from different tokamak devices.

In order to exemplify the type of plasmas obtained with the BSE regime, three discharges, #94442, #96994, and #97472, are compared to a typical type-I ELM discharge, #97395, in Fig. 2(left). All these

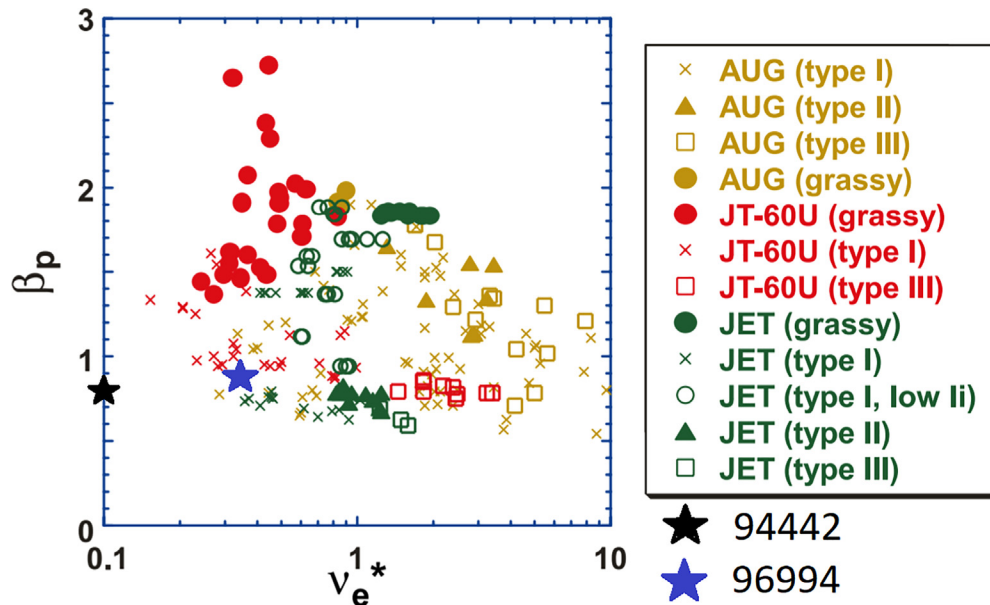**FIG. 1.** Comparison of the JET BSE discharges #94442 and #96994 with other small ELMs regimes in the diagram β_p vs ν_e^*. Reproduced with permission from Oyama *et al.*, Plasma Phys. Controlled Fusion **48**, A171 (2006). Copyright 2006 IOP Science.
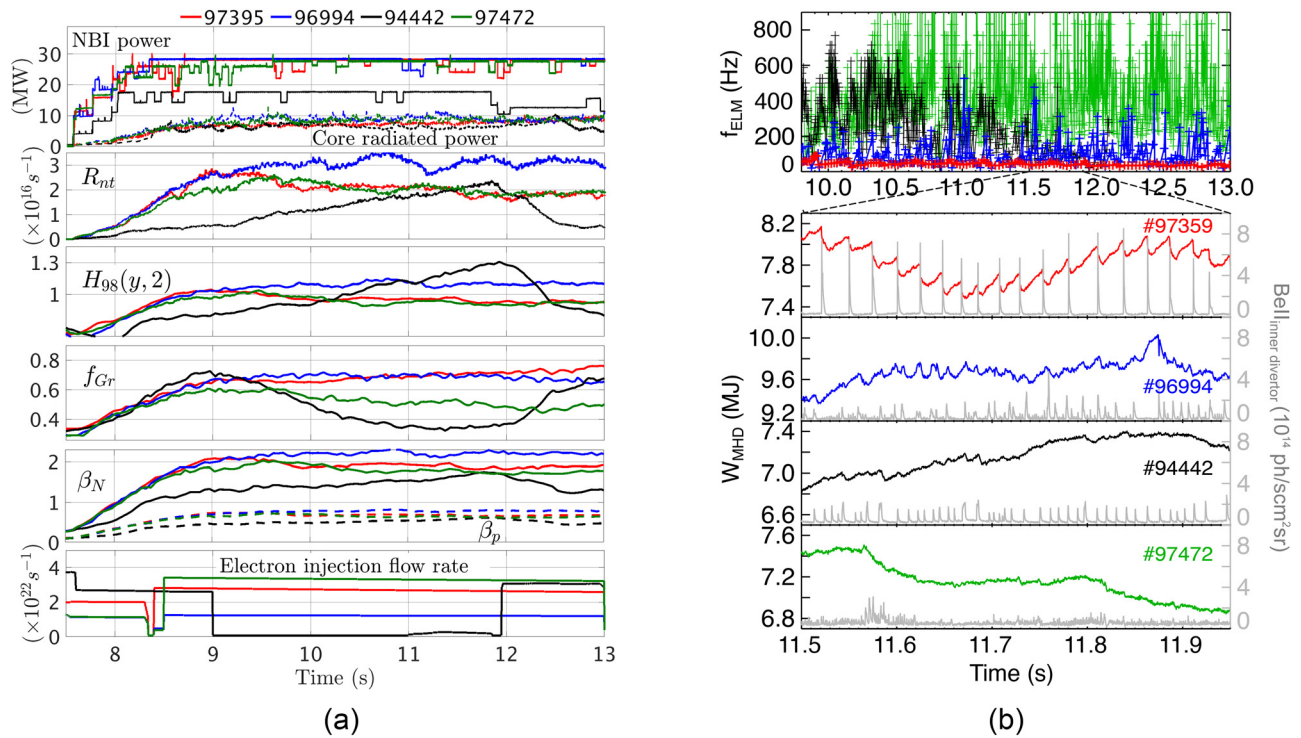
FIG. 2. Time evolution summary of the type I-ELM discharge #97395 and small ELMs discharges #94442 and #96994. $H_{98}(y,2)$ is defined as the thermal energy with respect to the energy from the IPB98 scaling.[37] $\beta_N = \beta a B_t / I_p [\%]$ with β the ratio between magnetic and thermal pressure. R_{nt} is the neutron rate from fusion reactions. f_{Gr} the ratio of the average density to the Greenwald density[38] (left). ELM frequency, total plasma energy W_{MHD}, and BeII line emission from the inner divertor for the discharges #97395, #96994, #94442, and #97472 (right).

discharges share a common configuration, with toroidal current, I_p = 3 MA, toroidal magnetic field, B_t = 2.8 T, q_{95} = 3.2, and a low triangularity configuration, δ = 0.23. In addition to the Neutral Beam Injection (NBI) heating, 4 MW of Ion Cyclotron Heating (ICRH) was applied to all the discharges. The pulses #97395, #96994, and #97472 have the same total input power, 32 MW; however, the particle source is provided in different ways. Whereas for the pulse #97395, the deuterium source is provided with a D gas puff, with a flux rate of $\Gamma_e(D) = 2.5 \times 10^{22}$ s^{-1}, in the case of #96994, it has a mixture of D gas puff at a reduced rate, $\Gamma_e(D) = 0.4 \times 10^{22}$ s^{-1}, Ne injection, $\Gamma_e(Ne) = 0.8 \times 10^{22}$ s^{-1}, and 2 mm D pacing pellets at frequency $f = 45$ Hz. Recent experiments in JET,[17] which studied the possibility of Ne as an external radiator impurity for ITER detachment conditions, showed that the size of ELMs is reduced with the injection of Ne. Therefore, the addition of small quantities of Ne was tested in some of the baseline plasmas discussed here. The quantity of Ne injected is small compared to the one used in highly radiating scenarios,[17,18] as otherwise the neutron rate can significantly decrease.[19] Unlike in the highly radiating scenarios mentioned above, the divertor remains attached in the BSE regime with Ne injection.

In the case of #97395, regular type-I ELMs at f_{ELM} = 45 Hz are obtained, with a relative average plasma energy loss during individual ELMs of $\Delta W_{ELM}/W_{MHD}$ = 2.2%. However, the discharge #96994 has a compound ELM behavior,[20] with isolated large ELMs followed by long periods of faster and smaller ELMs, with frequencies up to f_{ELM}

= 400 Hz, resulting in a significant reduction of the averaged energy ELM losses, $\Delta W_{ELM}/W_{MHD}$ = 0.8%, as shown in Fig. 2 (right). In terms of performance, #96994 performs better as both the thermal stored energy and neutron rate production are higher than the standard type-I ELMy H-mode #97395, although both have f_{Gr} = 0.7. Furthermore, in the discharge #96994, the total core radiated power remains steady with no impurity accumulation in the inner core, i.e., close to the plasma axis, unlike other high confinement scenarios at JET with type-I ELMs.[6] It is important to stress that, in terms of global parameters, the discharge #96994 is close to what it is expected for the inductive scenario in ITER,[8] $H_{98}(y,2)$ = 1.05, β_N = 2.1, β_p = 0.8, q_{95} = 3.2 with ν_e^* = 0.37.

The accessibility to high confinement small ELMs regimes is very broad. Such regime is also obtained specifically at zero gas injection, as shown in Fig. 2(left) for the discharge #94442, heated with 17 MW of NBI power and with no pellets or Ne injection. In this case, f_{ELM} reaches high values, varying from 600 to 100 Hz, and the size of ELM becomes so small that the drop in energy associated with single ELMs is within the noise level of the fast W_{MHD} signal ($\sim$50 kJ) resulting in a maximum estimated ELM energy loss of $\Delta W_{ELM}/W_{MHD}$ = 0.6%. The small ELMs obtained in the BSE scenarios are associated with an averaged ELM energy loss normalized to the pedestal energy (W_{Ped}) of $\Delta W_{ELM}/W_{Ped}$ = 3%–5% which, if achievable for plasma conditions that meet the requirements for the ITER Q = 10 operation, would be compatible with an acceptable divertor lifetime.[21]

The electron density continuously decreases after stopping the injection of neutral gas, reaching a stationary value of $F_{gr} = 0.3$ at $t = 11.4$ s. During the phase with no gas injected, $H_{98}(y, 2)$ and R_{nt} continuously increase, reaching values close to the discharge #97395, which is heated with more NBI power. No impurity accumulation in the plasma center is detected and ν_e^* reaches ITER expectations, $\nu_e^* = 0.1$.

The injection of Ne is shown to be beneficial for decreasing the size of ELMs and increasing their frequency. This is shown in Fig. 2(left) for the discharge #97472, which has increased Ne injection, $\Gamma_e(Ne) = 3 \times 10^{22}$ s^{-1}, compared to #96994. Clearly, the size of ELMs is reduced and their frequency has increased for the discharge #97472.

It is important to clarify how plasmas with BSE extrapolate to even higher I_p as high I_p will be the typical operational regime of ITER. This is studied by analyzing the discharge #96482 at $I_p = 3.5$ MA and $q_{95} = 3.2$ as shown in Fig. 3. The discharge #96482, with low neutral gas injection, $\Gamma_e(D) = 0.95 \times 10^{22}$ s^{-1}, and D pellets, has $H_{98}(y, 2) = 1.0$, $\beta_N = 1.8$ and $\beta_p = 0.6$ at much smaller ELM size and double neutron rate by D–D fusion reactions, R_{nt}, than the type-I ELM discharge #97395, which demonstrates that such small ELMs are compatible with high fusion power at high I_p. Since $\sim$50% of R_{nt} is due to DD thermonuclear reactions for the discharges discussed in this section, the fusion power obtained is a good representation of ITER conditions, which will be dominated by thermonuclear reactions.

CONFINEMENT AND PEDESTAL ANALYSES

A detailed study has been performed in order to clarify the physical mechanisms behind the onset of these small ELMs and the origin of good core confinement in the BSE regimes. Clear differences in the electron and ion temperatures, electron density, and rotation profiles are already evident as shown in Fig. 4. Notably, the ratio T_i/T_e, including at the pedestal top, and the toroidal rotation significantly increased for the cases with small ELMs. This is accompanied by a reduction of
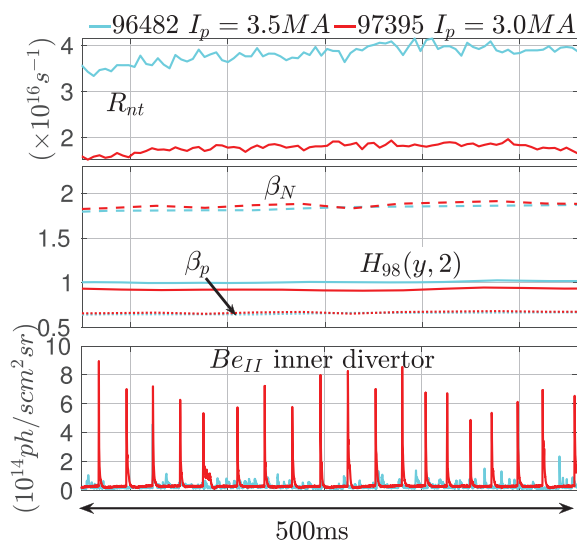
the density at the top of the pedestal. In particular, for the discharges #96994 and #97395, at the same power and therefore torque, the central density is nearly identical, whereas the density at the pedestal is 25% lower and core rotation is 36% higher at $\rho = 0.4$ for the pulse #96994, where ρ is the normalized toroidal flux. Such features show that momentum confinement is also improved with small ELMs, as it usually happens in JET plasmas with low gas fueling and pellet injection.[22]

Interestingly, the pedestal pressure remains nearly constant, at $P_{ped} = 34$ kPa for #96994 and $P_{ped} = 36$ kPa for #97395. Particularly striking are the differences in the pedestal structure. Both the electron density and temperature pedestals become wider, and there is a substantial reduction in the edge density gradient as the edge density decreases. Compared to #97395, where the pedestal top is located at $\rho = 0.94$, for the discharges with small ELMs, the pedestal top is located at $\rho = 0.91$.

A Peeling–Balling (P–B) analysis has been performed with the code MINERVA-DI,[23] which solves the extended Frieman–Rotenberg equation and includes rotation and diamagnetic effects, in order to study whether such MHD modes might be responsible for the onset of small ELMs. As shown in Fig. 5, the discharge #97395 is at the P–B boundary as expected from type-I ELMs; however, the small ELMs discharges tend to be farther from the P–B boundary and in the stable region, especially, for the pulse #94442, as a consequence of the reduced pressure gradient within the pedestal region. Such results indicate other mechanisms, rather than MHD, for the onset of such ELMs.

With the aim of clarifying whether changes on turbulence characteristics can play a role, linear local turbulence simulations have been performed at the pedestal top of the discharges #96994 and #97395 with the gyrokinetic code GENE,[24] which solves the gyrokinetic equation. The input parameters fed to GENE are shown in Table I. Such parameters summarize the main differences at the pedestal top between BSE and type-I ELM. Whereas $\hat{s}$ and R/L_{T_i} are significantly lower in the BSE case, T_i/T_e and R/L_{n_e} are higher. As shown in Fig. 4, for the discharge #97395, the turbulence spectrum is dominated by low wavenumber, $k_y < 0.5$, with k_y normalized to $\rho_s = c_s/\omega_{ci}$, where $c_s = (T_e/m_D)^{1/2}$ and $\omega_{ci} = (eB_T/m_D)$ with m_D the deuterium mass. Such modes, at high growth rate, γ, and frequency, ω, are identified as Kinetic Ballooning Modes (KBMs) which is one of the main instabilities limiting the pedestal pressure gradient.[25] However, for the discharge #96994, KBMs are fully stabilized, whereas modes rotating in the electron diamagnetic direction identified here as Microtearing modes (MTMs)[26] and Trapped Electron Modes (TEMs)[27,28] are dominant at low k_y with low γ, reflecting the strong change of turbulence characteristics in the new small ELM regime. The impact of the different levels of impurities in both discharges has been analyzed by removing the impurities from the simulations and adding the ions to the main ion specie. The simulations show that unlike for the type-I ELM pulse, the impact of impurities on γ is particularly important for the BSE case as they further destabilize MTM while strongly stabilize high k_y modes.

Although such linear local gyrokinetic analyses already indicate some profound differences in turbulence characteristics for BSE plasmas compared to type-I ELMs, further analyses involving nonlinear global gyrokinetic simulations are necessary in order to fully characterize BSE turbulence. This is left for future studies.
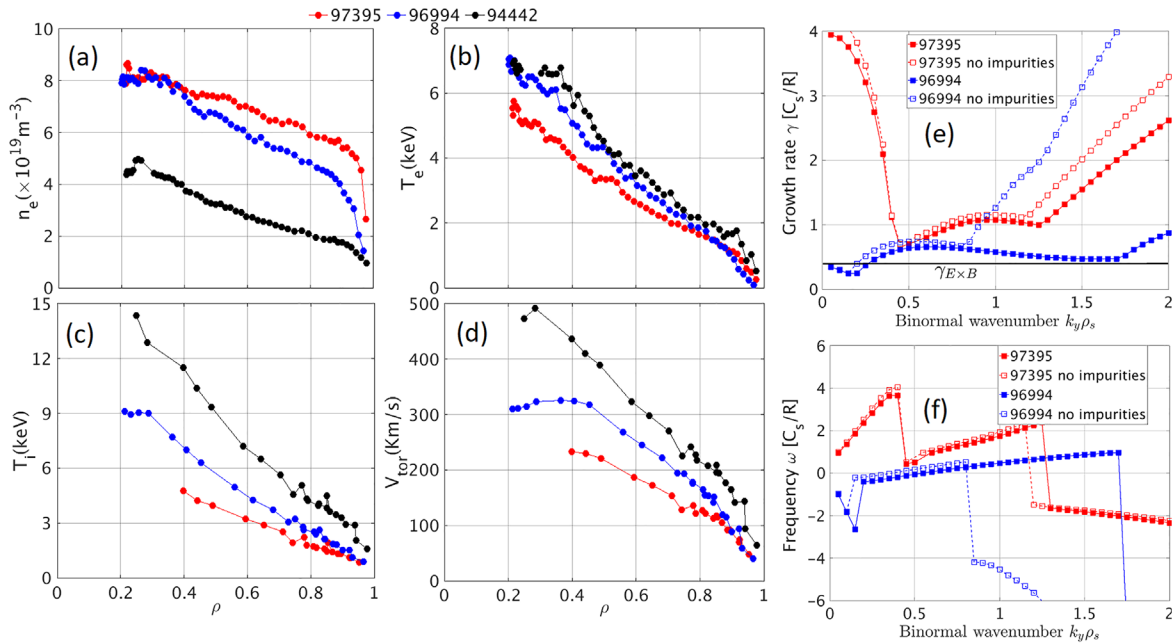

FIG. 3. Comparison between the small ELM discharge #96482 at $I_p = 3.5$ MA and the type-I ELM #97395 at $I_p = 3.0$ MA.

FIG. 4. Electron density (n_e) (a), electron temperature (T_e) (b), ion temperature (T_i) (c), and plasma toroidal rotation (V_{tor}) (d) for the discharges shown in Fig. 2 at t = 11.4 for #94442, t = 12 s for #97395, and t = 12.5 s for #96994. Turbulent growth rate, γ, (e) and frequency, ω, (f) for the discharges #97395 and #96994 at the top of the pedestal. γ and ω are in units of c_s/R, where $c_s = \sqrt{T_e/m_i}$ with T_e the electron temperature at the pedestal top and m_i the deuterium mass. The $E \times B$ shearing rate[39] (nearly identical for both discharges) is added in the same units for comparison.

IMPURITY BEHAVIOR ANALYSES

One key point of the plasmas in the BSE regime is the strong density peaking. Unlike previous JET results in high thermal confinement plasmas with type-I ELMs, which also lead to high density peaking during the stationary phase,[29] the plasmas with small ELMs

FIG. 5. P–B analysis[40] for the discharges #97395, #96994, and #94442.

analyzed in this work do not show any kind of stronger radiation pattern in the inner core region, at $\rho < 0.3$, as shown in the reconstructed bolometry 2D radiated power profiles for the discharges #94442 and #96994 in Fig. 6. Maximum radiation on the low field side of the outer plasma region is common in plasmas with low gas puff and pellets;[30] however, in the case of #96994, with the extrinsic impurity Ne injected, the radiation is redistributed toward a clear maximum at the divertor. No core impurity accumulation at $\rho < 0.3$ is detected. The impurity profiles, which that are calculated as explained in Ref. 31, clearly demonstrate that the main impurity in the inner core is Be, whereas high Z impurities, such as Ni and W, are either homogeneously distributed for the discharge #94442 or even have a hollow profile for #96994 with a maximum close to the pedestal as also shown in Fig. 6 and with an increase in Z_{eff} as shown in Fig. 7.

Usually, W is the main cause of the loss of plasma confinement and eventually radiation collapse in JET plasmas with high impurity accumulation close to the axis. The process of W accumulation is a complex process that depends on the strength of the W source on the plasma periphery and its transport. The analysis of the W source in the BSE regime could not be included here, since the ELM-resolved W production measurement used in JET is not reliable for the small ELMs (with $f_{ELM} > 100$ Hz) shown in this paper due to the low signal-to-noise ratio of the spectroscopy data used for this type of analysis. But it is worth noticing that analysis performed in JET has demonstrated that the W content of the plasma decreases with increasing ELM frequency, despite the fact that the W source can still increase with increasing ELM frequency (with the W source per ELM increasing with the ELM size, in terms of pedestal energy loss), demonstrating the efficacy of the ELM flushing in the control of the W impurity at
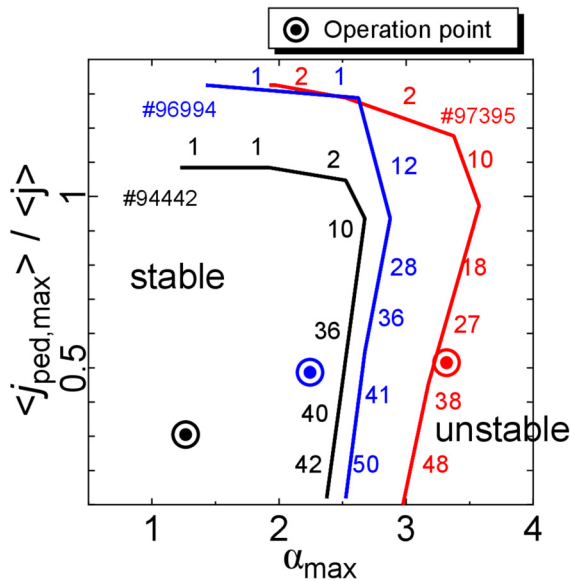
TABLE I. Employed plasma parameters in GENE simulations modeling at the pedestal top for the JET pulses #97395 at $t = 9.5$ s and #96994 at $t = 12.5$ s. q is the safety factor, $\hat{s}$ the magnetic shear, $L_{n_{e,i}} = -n_{e,i}/\nabla n_{e,i}$ with $n_{e,i}$ the electron and ion density, $L_{T_e} = -T_e/\nabla T_e$ with T_e the electron temperature, $L_{T_i} = -T_i/\nabla T_i$ with T_i the ion temperature, n_D is the deuterium density, n_{Be} is the beryllium density, n_{Ni} is the nickel density, and R is the plasma major radius.

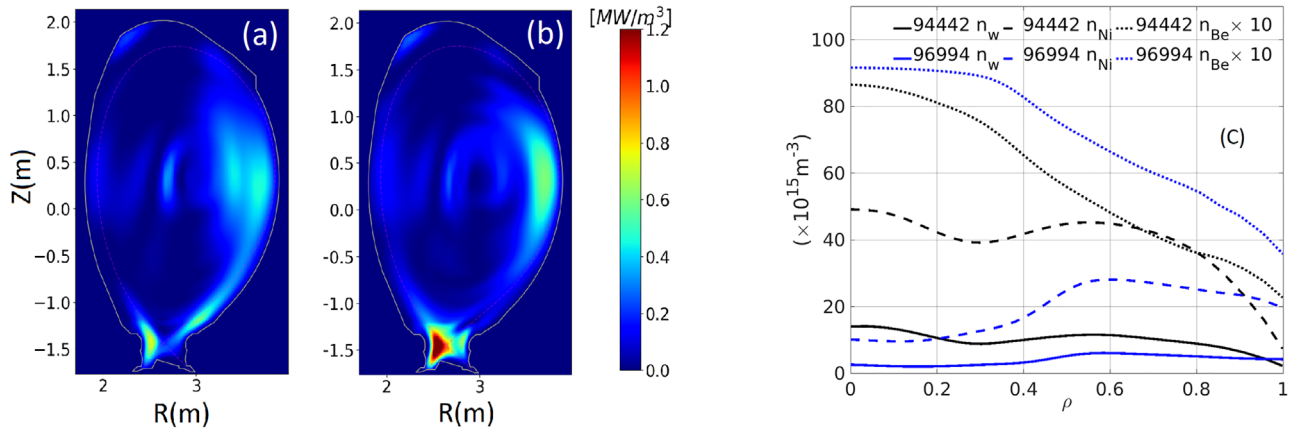| Shot No.	ρ	q	$\hat{s}$	T_i/T_e	$R/L_{n_{e,i}}$	R/L_{T_e}	R/L_{T_i}	n_D/n_e	n_{Be}/n_e	n_{Ni}/n_e
97395	0.94	3.1	2.3	1.0	3.6	16.6	19.0	0.92	1.8×10^{-2}	3.0×10^{-4}
96994	0.91	3.0	1.6	1.5	5.2	13.7	5.2	0.88	1.8×10^{-2}	1.6×10^{-3}

FIG. 6. Reconstructed bolometry 2D radiated power for the discharges #94442 (a) and #96994 (b). Tungsten (n_W), nickel (n_{Ni}), and beryllium (n_{Be}) density profiles for the discharges #94442 and #96994 (c).

the plasma edge.[32] This is a clear indication that in the conditions described in this paper, the W source plays a small role, and the focus has been in the exploration, via modeling, of the physics mechanism affecting the transport of W through the edge transport barrier, as well as in the core region. The transport of W from the periphery to the core plasma is mainly driven by the pinch term of the neoclassical transport which in conditions of high density peaking is usually

strongly inward.[6] W transport is analyzed in this paper by studying the neoclassical transport, in particular the convective part of the flux with the drift-kinetic code NEO.[33] As shown for the discharges #96994 and #94442 in Fig. 8, the W pinch is broadly positive (outward) for different plasma regions. Whereas for the discharge #94442, the outward W pinch is high at the pedestal top and significantly positive in the whole region $0.2 < \rho < 0.9$, for the discharge #96994, the outward W pinch is very strong in the region $0.2 < \rho < 0.65$, coinciding with the lack of radiation. Of particular importance is the role
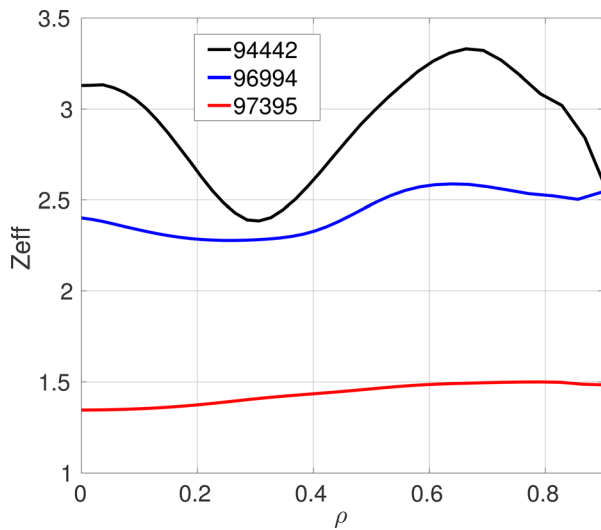

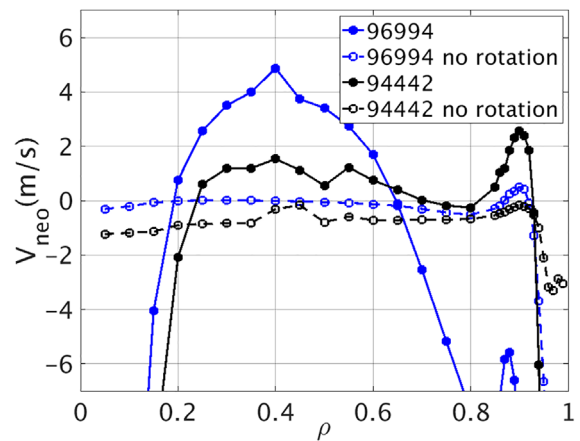**FIG. 7.** Zeff for the discharges #97395, #96994, and #94442.

FIG. 8. Convective pinch velocity (V_{neo}) for the discharges #94442 and #96994 including and excluding the toroidal rotation (positive is outward).

TABLE II. Employed plasma parameters in GENE simulations modeling at $\rho = 0.8$ for the JET pulses #97395 at $t = 9.5$ s, #96994 at $t = 12.5$ s, and #96482 at $t = 12.5$ s. n_{Ne} is the neon density.

Shot No.	ρ	q	$\hat{s}$	T_i/T_e	$R/L_{n_{e,i}}$	R/L_{T_e}	R/L_{T_i}	n_D/n_e	n_{Be}/n_e	n_{Ni}/n_e	n_W/n_e	n_{Ne}/n_e
97395	0.8	2.1	1.8	1.1	1.0	5.8	7.9	0.9	2.0×10^{-2}	2.0×10^{-4}	7.0×10^{-5}	0
96994	0.8	2.1	2.0	1.6	2.5	5.6	5.2	0.8	1.0×10^{-2}	4.9×10^{-4}	9.8×10^{-5}	1.0×10^{-2}
96482	0.8	2.1	1.8	1.5	2.4	5.6	6.6	0.8	4.0×10^{-2}	4.0×10^{-4}	1.0×10^{-4}	0

of rotation as it reverses the pinch from negative to positive, despite the fact that plasmas 2D asymmetries by means of centrifugal forces tend to increase the inward W pinch.[6] Therefore, for the first time at JET, it has been shown that high confinement plasmas can be inherently resilient to strong inner W accumulation, as expected in ITER.[34]

TURBULENCE AND TRANSPORT ANALYSES

A detailed core turbulence analysis has been performed using the GENE code in order to evaluate the origin of the high core confinement in the BSE regime. The analysis is focused at the radial location $\rho = 0.8$ as it is found that the main differences between small ELMs and type-I ELMs plasmas have their origin at the plasma edge. The input data fed to the GENE code are shown in Table II. The results of linear simulations for the pulse #96994 are shown in Fig. 9. Turbulence is dominated by the Ion Temperature Gradient (ITG),[35] mainly driven by the steep thermal ion temperature gradient. Electron Temperature Gradient (ETG) modes,[27] are also identified at smaller spatial scales. Several mechanisms play a role in the good confinement. When impurities located at such radial location, Be, Ni, W, and Ne, are taken into account, there is a reduction of γ_{max} of 40%. This shows that the edge-located impurities, blocked by the positive pinch from

neoclassical transport, have a beneficial effect on reducing transport driven by turbulence. In addition, a linear simulation has been performed for the pulses by artificially decreasing the experimental value of T_i/T_e, shown in Table II, to 1.00. The effect on γ_{max} is massive, with an increase of 33%. This feature points out to the important role of the pedestal, for which $T_i/T_e = 1.50$, as a source of core improved confinement. This is because the high values of T_i/T_e at the pedestal top propagate to the core and significantly contribute to the core's reduced turbulence.

The role of $E \times B$ shearing, which is known to reduce or even suppress ITG transport,[36] has also been analyzed for the discharge #96994 by means of nonlinear local simulations performed at $\rho = 0.8$. The method to calculate the heat flux from these nonlinear simulations and the definition of $E \times B$ shearing in GENE are specified in the Appendix. As shown in Fig. 9, the effect of $E \times B$ shearing leads to a reduction of the deuterium diffusivities by three to four times. Such effect, in addition to the localized edge impurities (including Ne) and the high T_i/T_e ratio starting at the pedestal, can explain the good core confinement obtained in the small ELMs plasmas. The same type of behavior is found for the discharge #94442 and, in general, for all the discharges with BSE.
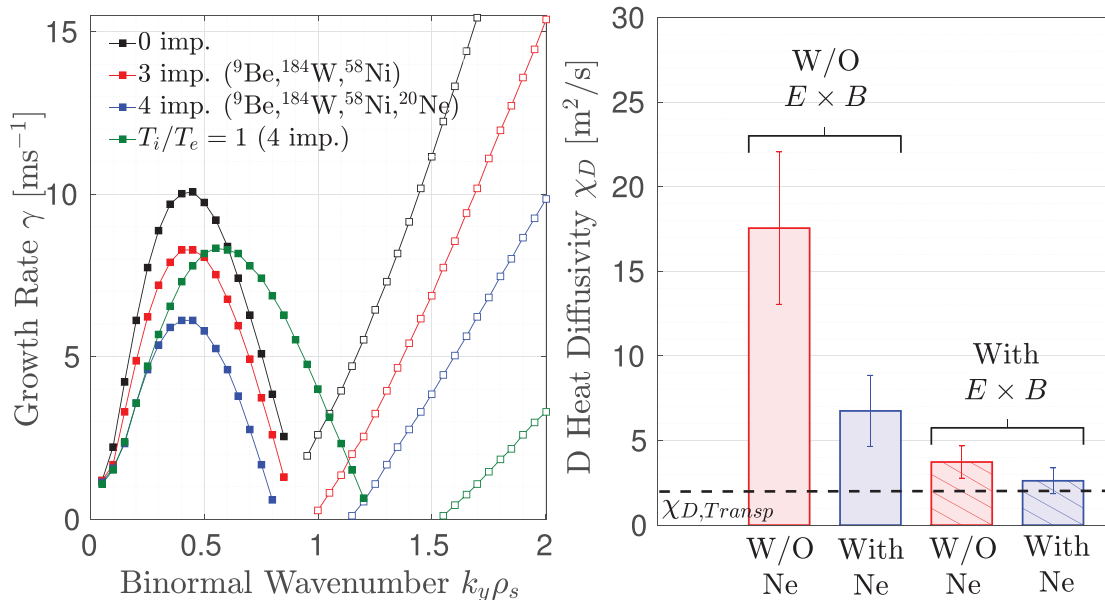

FIG. 9. Turbulence growth rates obtained with the GENE code for the discharge #96994. Solid symbols represent ITG modes, whereas empty symbols represent ETG modes (left) D heat diffusivity obtained from nonlinear simulations for the discharge #96994. The dashed line represents the D heat diffusivity calculated from the power balance in TRANSP (right).
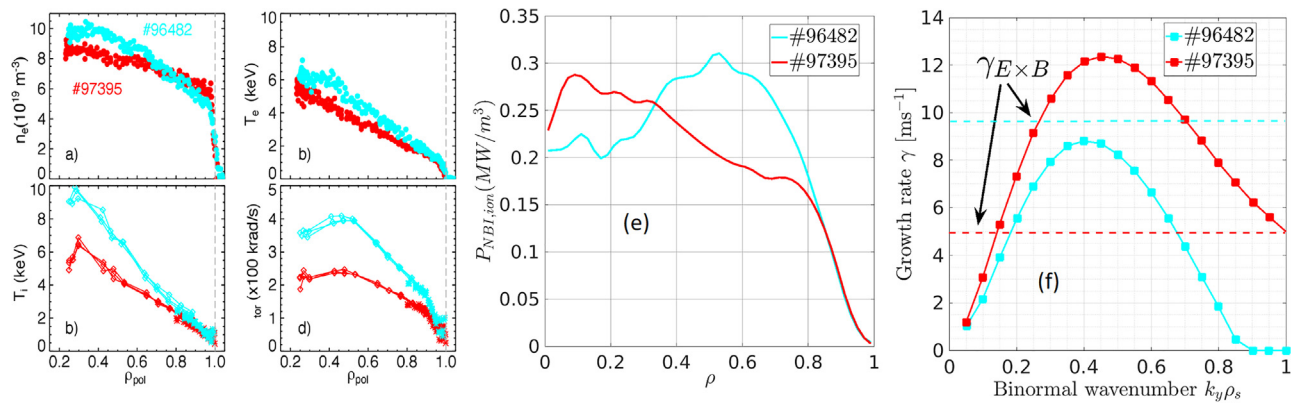
FIG. 10. Electron density (n_e) (a), electron temperature (T_e) (b), ion temperature (T_i) (c), and plasma toroidal rotation (V_{tor}) (d) at $t = 12$ s for #97395 and $t = 12.5$ s for #96482. NBI power transferred to the thermal ions (e). Turbulence growth rates obtained with the GENE code at $\rho = 0.8$. The dashed lines represent the $\gamma_{E \times B}$ for each discharge (f).

The impact of the ion heating source on the good confinement characteristics of BSE plasmas is investigated by comparing the high performance discharge #96482 at 3.5 MA with small ELMs and the type-I ELMy plasma #97395. From the comparison of the main profiles for both discharges shown in Fig. 10, it is clearly seen that for the #96482 pulse the typical characteristics of the BSE regime appear, i.e., high T_i/T_e, rotation and density peaking. Compared to the pulse #97395, the electron density at the pedestal is lower for #96482; however, since the density peaking is higher, the density at the inner core, i.e., at $\rho < 0.3$ is higher. Such a difference in density has an impact on the NBI beam penetration. In Fig. 10, the NBI ion heating, calculated with TRANSP for both discharges, is shown. The ion heating is lower close to the plasma axis for the discharge in the BSE regime, and yet, the ion temperature is much higher than the type-I ELM pulse. We speculate that rather than ion heating, transport and turbulence might be more important for the determination of T_i in BSE plasmas. This is studied with gyrokinetic linear simulations performed for both discharges with the GENE code at $\rho = 0.8$, including three impurities. Clearly, γ_{max} is higher for the discharge #97395 than for #96482, indicating higher turbulence levels which in addition coexist with lower values of $\gamma_{E \times B}$ for #97395. Overall, clear differences on turbulence characteristics are found for the BSE core plasmas compared to type-I ELMs; however, more analyses are required to fully characterize the new BSE regime.

DISCUSSION AND CONCLUSIONS

The results discussed in this paper show a new high performance H-mode regime with small ELMs, called BSE, found at JET covering a novel physics phase space at $q_{95} \sim 3$, $\beta_p < 1$ and low pedestal collisionality, as expected in ITER baseline conditions. Such an operational regime is obtained by controlling and optimizing the particle fueling at high input power, current, and magnetic field. This triggers an optimum self-organized plasma state characterized by simultaneously accessing small ELMs and high fusion power and confinement and no impurity accumulation. The edge reduction of turbulent transport, the increase in rotation, and the reverse of impurity convection from inward to outward are key physical mechanisms that spontaneously lead to such a state.

Very high thermal confinement, $H_{98}(y, 2) \sim 1.4$, is obtained in BSE in a nonstationary way when the injected gas fueling is fully removed and $f_{Gr} \sim 0.3$. This kind of plasma is not the one expected in ITER; however, it shows that pedestals with low particle sources by gas injection can behave in a very different way compared to type-I ELMs as a result of the large pedestal width, which makes the pedestal stable to P–B modes in the BSE regime.

Stationary plasmas are obtained when the gas injection is partially replaced by pacing D pellets and $f_{Gr} \sim 0.7$, which is close to what it is expected in ITER. In such conditions, the neutron rate and thermal confinement can be similar or even higher than for type-I ELMs at the same input power, which indicates that small ELMs plasmas are adequate for high fusion power generation in metallic wall devices.

The full applicability of this new regime requires further studies in conditions closer to those expected in ITER and which are difficult to attain at JET. Notably, BSE needs to be studied in the presence of strong electron heating and reduced torque. In addition, the power width dependence in the Scrape-Off Layer (SOL) in plasmas with BSE should require extended studies as it is a key point for ITER. Regarding high triangularity, semi-detached or fully detached plasmas, initial results at JET using high heating power (30 MW) and Ne seeding in high triangularity plasmas show that plasmas in such conditions are prone to developing small ELMs and high confinement.[17] The future JET scientific program will further explore such a route.

Nevertheless, the results shown in this paper already open up the possibility that magnetically confined plasmas in large scale fusion devices self-organize in the direction required for optimum fusion power generation, meanwhile strong heat fluxes to the plasma-facing components are avoided. However, it is unclear yet whether the high levels of separatrix and SOL densities, necessary for power exhaust, are compatible with the newly explored BSE scenario. This will be a topic for future research at JET.

ACKNOWLEDGMENTS

AUTHOR DECLARATIONS
Conflict of Interest

The authors have no conflicts to disclose.

DATA AVAILABILITY

The data that support the findings of this study are available from the corresponding author upon reasonable request.

APPENDIX: DEFINITION OF GENE OBSERVABLES

The normalized perpendicular $E \times B$ shearing is defined in GENE as

$$\gamma_{E \times B} = (r/q)(d\Omega/dr)/(c_s/a),$$

where q is the local value of the safety factor, r the radial coordinate, Ω the toroidal angular velocity, $c_s = \sqrt{(T_e/m_i)}$, and a the minor radius.

The heat flux for each specie s is defined in GENE as

$$\langle Q_s \rangle = \left\langle \int d^3 v \frac{1}{2} m_s v^2 f_s(\mathbf{x}, \mathbf{v}) \mathbf{v}_{E \times B}(\mathbf{x}) \right\rangle,$$

where $\mathbf{x} = (x, y, z)$ and $\mathbf{v} = (v_\parallel, \mu)$, $\langle \cdot \rangle$ denotes the flux-surface average, $f_s(\mathbf{x}, \mathbf{v})$ is the distribution function, $\mathbf{v}_{E \times B} = \frac{c}{B_0^2} \mathbf{B}_0 \times \nabla \bar{\bar{\xi}}$ is the generalized $E \times B$ drift velocity, with $\bar{\bar{\xi}} = \bar{\phi} - \frac{v_\parallel}{c} \bar{A}_\parallel + \frac{\mu}{q_s} \bar{B}_\parallel$ the gyroaveraged modified potential (in which q_s is the charge and the upper bar indicating a gyroaveraged quantity), and the subscript s refers to the species.

REFERENCES

[1]M. Shimada, D. Campbell, V. Mukhovatov, M. Fujiwara, N. Kirneva, K. Lackner, M. Nagami, V. Pustovitov, N. Uckan, J. Wesley, N. Asakura, A. Costley, A. Donné, E. Doyle, A. Fasoli, C. Gormezano, Y. Gribov, O. Gruber, T. Hender, W. Houlberg, S. Ide, Y. Kamada, A. Leonard, B. Lipschultz, A. Loarte, K. Miyamoto, V. Mukhovatov, T. Osborne, A. Polevoi, and A. Sips, "Chapter 1: Overview and summary," Nucl. Fusion **47**, S1 (2007).

[2]F. Wagner, G. Fussmann, T. Grave, M. Keilhacker, M. Kornherr, K. Lackner, K. McCormick, E. R. Müller, A. Stäbler, G. Becker, K. Bernhardi, U. Ditte, A. Eberhagen, O. Gehre, J. Gernhardt, G. v Gierke, E. Glock, O. Gruber, G. Haas, M. Hesse, G. Janeschitz, F. Karger, S. Kissel, O. Klüber, G. Lisitano, H. M. Mayer, D. Meisel, V. Mertens, H. Murmann, W. Poschenrieder, H. Rapp, H. Röhr, F. Ryter, F. Schneider, G. Siller, P. Smeulders, F. Söldner, E. Speth, K. H. Steuer, Z. Szymanski, and O. Vollmer, "Development of an edge transport barrier at the H-mode transition of ASDEX," Phys. Rev. Lett. **53**, 1453 (1984).

[3]H. Zohm, "Edge localized modes (ELMs)," Plasma Phys. Controlled Fusion **38**, 105 (1996).

[4]O. Gruber, A. Sips, R. Dux, T. Eich, J. Fuchs, A. Herrmann, A. Kallenbach, C. Maggi, R. Neu, T. Pü4tterich, J. Schweinzer, J. Stober, and ASDEX Upgrade Team, "Compatibility of ITER scenarios with full tungsten wall in ASDEX Upgrade," Nucl. Fusion **49**, 115014 (2009).

[5]R. Neu, G. Arnoux, M. Beurskens, V. Bobkov, J. B. G. C. S. Brezinsek, C. Challis, J. W. Coenen, E. de la Luna, and R. D. P. C. de Vries, "First operation with the jet international thermonuclear experimental reactor-like wall," Phys. Plasmas **20**, 056111 (2013).

[6]C. Angioni, P. Mantica, T. Pütterich, M. Valisa, M. Baruzzo, E. Belli, P. Belo, F. Casson, C. Challis, P. Drewelow, C. Giroud, N. Hawkes, T. Hender, J. Hobirk, T. Koskela, L. L. Taroni, C. Maggi, J. Mlynar, T. Odstrcil, M. Reinke, and M. Romanelli, "Tungsten transport in JET H-mode plasmas in hybrid scenario, experimental observations and modelling," Nucl. Fusion **54**, 083028 (2014).

[7]X. Litaudon, S. Abduallev, M. Abhangi, P. Abreu, M. Afzal, K. M. Aggarwal, T. Ahlgren, J. H. Ahn, L. Aho-Mantila, N. Aiba et al., "Overview of the JET results in support to ITER," Nucl. Fusion **57**, 102001 (2017).

[8]A. Sips, J. Schweinzer, T. Luce, S. Wolfe, H. Urano, J. Hobirk, S. Ide, E. Joffrin, C. Kessel, S. Kim, P. Lomas, I. Nunes, T. Pütterich, F. Rimini, W. Solomon, J. Stober, F. Turco, and P. de Vries, "Assessment of the baseline scenario at q 95 ~ 3 for ITER," Nucl. Fusion **58**, 126010 (2018).

[9]Y. Kamada, T. Oikawa, L. Lao, T. Takizuka, T. Hatae, A. Isayama, J. Manickam, M. Okabayashi, T. Fukuda, and K. Tsuchiya, "Disappearance of giant ELMs and appearance of minute grassy ELMs in JT-60U high-triangularity discharges," Plasma Phys. Controlled Fusion **42**, A247 (2000).

[10]J. Stober, M. Maraschek, G. Conway, O. Gruber, A. Herrmann, A. Sips, W. Treutterer, H. Zohm, and ASDEX Upgrade Team, "Type II ELMy H modes on ASDEX Upgrade with good confinement at high density," Nucl. Fusion **41**, 1123 (2001).

[11]J. Stober, P. Lomas, G. Saibene, Y. Andrew, P. Belo, G. Conway, A. Herrmann, L. Horton, M. Kempenaars, H.-R. Koslowski, A. Loarte, G. Maddison, M. Maraschek, D. McDonald, A. Meigs, P. Monier-Garbet, D. Mossessian, M. Nave, N. Oyama, V. Parail, C. Perez, F. Rimini, R. Sartori, A. Sips, P. Thomas, Contributors to the EFDA-JET Workprogramme, and ASDEX Upgrade Team, "Small ELM regimes with good confinement on JET and comparison to those on ASDEX Upgrade, Alcator C-mod and JT-60U," Nucl. Fusion **45**, 1213 (2005).

[12]N. Oyama, P. Gohil, L. D. Horton, A. E. Hubbard, J. W. Hughes, Y. Kamada, K. Kamiya, A. W. Leonard, A. Loarte, R. Maingi, G. Saibene, R. Sartori, J. K. Stober, W. Suttrop, H. Urano, W. P. West, and ITPA Pedestal Topical Group, "Pedestal conditions for small ELM regimes in tokamaks," Plasma Phys. Controlled Fusion **48**, A171 (2006).

[13]E. Viezzer, "Access and sustainment of naturally ELM-free and small-ELM regimes," Nucl. Fusion **58**, 115002 (2018).

[14]P. Lang, G. Conway, T. Eich, L. Fattorini, O. Gruber, S. Günter, L. Horton, S. Kalvin, A. Kallenbach, M. Kaufmann, G. Kocsis, A. Lorenz, M. Manso, M. Maraschek, V. Mertens, J. Neuhauser, I. Nunes, W. Schneider, W. Suttrop, H. Urano, and ASDEX Upgrade Team, "ELM pace making and mitigation by pellet injection in ASDEX Upgrade," Nucl. Fusion **44**, 665 (2004).

[15]G. S. Xu, Q. Q. Yang, N. Yan, Y. F. Wang, X. Q. Xu, H. Y. Guo, R. Maingi, L. Wang, J. P. Qian, X. Z. Gong, V. S. Chan, T. Zhang, Q. Zang, Y. Y. Li, L. Zhang, G. H. Hu, and B. N. Wan, "Promising high-confinement regime for steady-state fusion," Phys. Rev. Lett. **122**, 255001 (2019).

[16]N. Oyama, Y. Sakamoto, A. Isayama, M. Takechi, P. Gohil, L. Lao, P. Snyder, T. Fujita, S. Ide, Y. Kamada, Y. Miura, T. Oikawa, T. Suzuki, H. Takenaga, K. Toi, and JT-60 Team, "Energy loss for grassy ELMs and effects of plasma rotation on the ELM characteristics in JT-60U," Nucl. Fusion **45**, 871 (2005).

[17]C. Giroud, "High performance ITER-baseline discharges in deuterium with nitrogen and neon-seeding in the JET-ILW," in 28th IAEA Fusion Energy Conference (FEC 2020) (2021).

[18]S. Glöggler, M. Wischmeier, E. Fable, E. Solano, M. Sertoli, M. Bernert, G. Calabrò, M. Chernyshova, A. Huber, E. Kowalska-Strzeciwilk, C. Lowry, E. de la Luna, C. Maggi, U. Stroth, H. Sun, M. Reinke, S. Wiesen, and JET Contributors, "Characterisation of highly radiating neon seeded plasmas in JET-ILW," Nucl. Fusion **59**, 126031 (2019).

[19]C. Challis, E. Belonohy, A. Czarnecka, D. Frigione, C. Giroud, J. Graves, J. Hobirk, A. Huber, E. Joffrin, N. Krawczyk, M. Lawson, M. Mantsinen, K. McClements, T. O'Gorman, S. Silburn, A. Sips, E. Solano, and JET Contributors, "Impact of neon seeding on fusion performance in JET ILW hybrid plasmas," in 44th EPS Conference on Plasma Physics (IEEE, 2017), p. P2.153.

[20]L. Garzotti, C. Challis, R. Dumont, D. Frigione, J. Graves, E. Lerche, J. Mailloux, M. Mantsinen, F. Rimini, F. Casson, A. Czarnecka, J. Eriksson, R. Felton, L. Frassinetti, D. Gallart, J. Garcia, C. Giroud, E. Joffrin, H.-T. Kim, N. Krawczyk, M. Lennholm, P. Lomas, C. Lowry, L. Meneses, I. Nunes, C. Roach, M. Romanelli, S. Sharapov, S. Silburn, A. Sips, E. Stefániková, M. Tsalas, D. Valcarcel, M. Valovič, and JET Contributors, "Scenario development for D–T operation at JET," Nucl. Fusion **59**, 076037 (2019).

[21]A. Loarte, G. Saibene, R. Sartori, V. Riccardo, P. Andrew, J. Paley, W. Fundamenski, T. Eich, A. Herrmann, G. Pautasso, A. Kirk, G. Counsell, G. Federici, G. Strohmayer, D. Whyte, A. Leonard, R. A. Pitts, I. Landman, B. Bazylev, and S. Pestchanyi, "Transient heat loads in current fusion experiments, extrapolation to ITER and consequences for its operation," Phys. Scr. **2007**(T128), 222.

[22]H.-T. Kim, A. Sips, M. Romanelli, C. Challis, F. Rimini, L. Garzotti, E. Lerche, J. Buchanan, X. Yuan, S. Kaye, and JET Contributors, "High fusion performance at high Ti/Te JET-ILW baseline plasmas with high NBI heating power and low gas puffing," Nucl. Fusion **58**, 036020 (2018).

[23]N. Aiba, M. Honda, and K. Kamiya, "Impact of ion diamagnetic drift on MHD stability at edge pedestal in JT-60U rotating plasmas," Nucl. Fusion **57**, 022011 (2016).

[24]F. Jenko, W. Dorland, M. Kotschenreuther, and B. N. Rogers, "Electron temperature gradient driven turbulence," Phys. Plasmas **7**, 1904 (2000).

[25]P. Snyder, N. Aiba, M. Beurskens, R. Groebner, L. Horton, A. Hubbard, J. Hughes, G. Huysmans, A. K. Y. Kamada, C. Konz, A. Leonard, J. Lonnroth, C. Maggi, T. O. R. Maingi, N. Oyama, A. Pankin, S. Saarelma, G. Saibene, J. Terry, H. Urano, and H. Wilson, "Pedestal stability comparison and ITER pedestal prediction," Nucl. Fusion **49**, 085035 (2009).

[26]X. Garbet, F. Mourgues, and A. Samain, "Non-linear self-consistency of microtearing modes," Plasma Phys. Controlled Fusion **30**, 343 (1988).

[27]W. Horton, "Drift waves and transport," Rev. Mod. Phys. **71**, 735 (1999).

[28]X. Garbet, P. Mantica, C. Angioni, E. Asp, Y. Baranov, C. Bourdelle, R. Budny, F. Crisanti, G. Cordey, L. Garzotti, N. Kirneva, D. Hogeweij, T. Hoang, F. Imbeaux, E. Joffrin, X. Litaudon, A. Manini, D. C. McDonald, H. Nordman, V. Parail, A. Peeters, F. Ryter, C. Sozzi, M. Valovic, T. Tala, A. Thyagaraja, I. Voitsekhovitch, J. Weiland, H. Weisen, A. Zabolotsky, and JET EFDA Contributors, "Physics of transport in tokamaks," Plasma Phys. Controlled Fusion **46**, B557 (2004).

[29]F. Casson, H. Patten, C. Bourdelle, S. Breton, J. Citrin, F. Koechl, M. Sertoli, C. Angioni, Y. Baranov, R. Bilato, E. Belli, C. Challis, G. Corrigan, A. Czarnecka, O. Ficker, L. Frassinetti, L. Garzotti, M. Goniche, J. Graves, T. Johnson, K. Kirov, P. Knight, E. Lerche, M. Mantsinen, J. Mylnar, M. Valisa, and JET Contributors, "Predictive multi-channel flux-driven modelling to optimise ICRH tungsten control and fusion performance in JET," Nucl. Fusion **60**, 066029 (2020).

[30]J. R. Field, S. Aleiferis, É. Belonohy, P. Carvalho, I. Coffey, D. Frigione, L. Garzotti, L. Horvath, H.-T. Kim, M. Lennholm, E. Lerche, P. Lomas, C. G. Lowry, J. Mailloux, F. Rimini, C. M. Roach, M. Sertoli, Ž. Štancar, G. Szepesi, and D. Van Eester, "The impact of fuelling and w radiation on the performance of high-power, ITER-baseline scenario plasmas in JET-ILW," Plasma Phys. Controlled Fusion **63**, 095013 (2021).

[31]M. Sertoli, P. J. Carvalho, C. Giroud, and S. Menmuir, "Measuring the plasma composition in tokamaks with metallic plasma-facing components," J. Plasma Phys. **85**, 905850504 (2019).

[32]N. D. Harder, S. Brezinsek, T. Pütterich, N. Fedorczak, G. Matthews, A. Meigs, M. Stamp, M. van de Sanden, G. V. Rooij, and JET Contributors, "ELM-resolved divertor erosion in the JET ITER-like wall," Nucl. Fusion **56**, 026014 (2016).

[33]E. A. Belli and J. Candy, "Kinetic calculation of neoclassical transport including self-consistent electron and impurity dynamics," Plasma Phys. Controlled Fusion **50**, 095010 (2008).

[34]R. Dux, A. Loarte, E. Fable, and A. Kukushkin, "Transport of tungsten in the H-mode edge transport barrier of ITER," Plasma Phys. Controlled Fusion **56**, 124003 (2014).

[35]F. Romanelli, "Ion temperature-gradient-driven modes and anomalous ion transport in tokamaks," Phys. Fluids B **1**, 1018 (1989).

[36]E. Doyle, W. Houlberg, Y. Kamada, V. Mukhovatov, T. Osborne, A. Polevoi, G. Bateman, J. Connor, J. Cordey, T. Fujita, X. Garbet, T. Hahm, L. Horton, A. Hubbard, F. Imbeaux, F. Jenko, J. Kinsey, Y. Kishimoto, J. Li, T. Luce, Y. Martin, M. Ossipenko, V. Parail, A. Peeters, T. Rhodes, J. Rice, C. Roach, V. Rozhansky, F. Ryter, G. Saibene, R. Sartori, A. Sips, J. Snipes, M. Sugihara, E. Synakowski, H. Takenaga, T. Takizuka, K. Thomsen, M. Wade, H. Wilson, and ITPA Transport Physics Topical Group, ITPA Confinement Database and Modelling Topical Group and ITPA Pedestal Edge Topical Group, "Chapter 2: Plasma confinement and transport," Nucl. Fusion **47**, S18 (2007).

[37]ITER Physics Expert Group on Confinement Transport and ITER Physics Expert Group on Confinement Modelling and Database, and ITER Physics Basis Editors, "Chapter 2: Plasma confinement and transport," Nucl. Fusion **39**, 2175 (1999).

[38]M. Greenwald, "Density limits in toroidal plasmas," Plasma Phys. Controlled Fusion **44**, R27 (2002).

[39]T. S. Hahm and K. H. Burrell, "Flow shear induced fluctuation suppression in finite aspect ratio shaped tokamak plasma," Phys. Plasmas **2**, 1648 (1995).

[40]P. Snyder, H. Wilson, J. Ferron, L. Lao, A. Leonard, D. Mossessian, M. Murakami, T. Osborne, A. Turnbull, and X. Xu, "ELMs and constraints on the H-mode pedestal: Peeling–ballooning stability calculation and comparison with experiment," Nucl. Fusion **44**, 320 (2004).